Progress In Electromagnetics Research C, Vol. 115, 277–289, 2021

Artificial Neural Network Based SIW Bandpass Filter Design Using Complementary Split Ring Resonators

Ranjit Kumar Rayala* **and Raghavan Singaravelu**

Abstract—A novel Artificial Neural Network (ANN) based two Substrate integrated waveguide (SIW) bandpass filters comprising Complementary Split Ring Resonators (CSRRs) are proposed in this paper. These CSRRs are modelled on the upper layer of the SIW cavity. A feed forward multilayer perceptron (FF-MLP) neural network is used to optimize the physical dimensions of the proposed filters. To validate the analytical results, physical prototypes of the proposed filters are fabricated, and a measurement is carried out with a Combinational Network Analyzer (Anritsu-MS2037C), and the obtained experimental results agree well with the estimated results using full wave analysis. Within the passband from 8.22 to 8.95 GHz, S_{12} of the first filter shows better than -0.5 dB insertion loss (IL) and a fractional bandwidth of 8.5%, and within the passband from 8.21 to 8.73 GHz, the second filter shows IL about -0.8 dB and a fractional bandwidth of 6.1%.

1. INTRODUCTION

Substrate Integrated Waveguide (SIW) filters have recently attracted a lot of attention because of their high efficiency, easy fabrication process with simple printed circuit board (PCB) technology, small size, low insertion loss, high selectivity, and ease of integration with microwave and millimetre wave circuits [1, 2]. In modern communication systems, one of the important requirements is miniaturization. SIW bandpass filter has been designed and investigated using slow wave method [3, 4]. SIW structures are typically composed of conducting vias which are placed in a dielectric substrate that connects two parallel metal plates, enabling the use of traditional rectangular waveguide components in planar form. The conventional PCB technique can be used in SIW based passive, active devices, microwave components, and antennas. The latest developments in SIW technology in terms of its modelling, design, and technological implementation of SIW structures and components have been reported [5–8]. To acquire compact size and modular geometry, a new type of quasi-elliptic pass-band filters based on mushroom-shaped metallic resonators in SIW technology has been proposed [9]. SIW bandpass filter with a cross-shaped cavity that realizes six symmetrically simulated modes out of first eight higher order resonant modes has been proposed [10]. An SIW band-pass filter having wide and sharp stop band, which differs from filters with a direct coupling between input and output has been proposed [11]. An SIW bandpass filter, modelled on a double layer dielectric substrate consisting of metallic via holes in order to realize the classical H-plane filter has been proposed [12]. Two cascaded mushroom resonators have been modelled on the SIW cavity that works as a dual band bandpass filter has been presented [13]. On the waveguide top metal layer, a number of cross-slot patterns have been modelled to act as dual mode SIW filters [14].

The performance of SIW filters can be improved by using some special types of electromagnetic topologies like split ring resonator (SRR) and complementary split ring resonator (CSRR) and have been

Received 23 July 2021, Accepted 19 September 2021, Scheduled 9 October 2021

* Corresponding author: Ranjit Kumar Rayala (ranjit.rayala@gmail.com).

The authors are with the Department of Electronics and Communication Engineering, National Institute of Technology Tiruchirappalli, Trichy 620015, India.

adapted into SIW technology [15]. A novel diamond-shaped CSRR has been proposed and investigated based on an SIW bandpass filter [16]. An extended doublet bandpass filter that uses an SIW cavity with CSRRs on the top layer has been proposed, and a single layer bandpass filter with two transmission zeros (TZ) was analyzed [17]. An SIW filter with square CSRRs has been proposed, and the characteristics of passband have been observed by varying the directions of the CSRRs [18]. CSRR has been modelled on the top surface of the SIW that provides a passband below the initial cutoff frequency of the waveguide TE_{10} mode [19]. By loading CSRRs onto the SIW cavity, the SIW bandpass filters have been achieved in compact size and high selectivity [20]. A double sided CSRR half mode SIW filter that provides lower resonant frequency than the conventional model because of the coupling effect between CSRRs of the upper and lower plates has been proposed [21]. Based on evanescent-mode propagation, a compact SIW bandpass filter using broad side coupled CSRR [22] and fractal open complementary split-ring resonators (FOCSRRs) unit-cell has been presented [23]. Complementary open-ring resonators (CORRs) loaded half mode substrate integrated waveguide (HMSIW), with many transmission zeros and wide stopband, have been proposed [24]. Novel dual mode SIW filters that can provide multiple transmission zeros have been proposed [25].

One of the issues with designing SIW components and RF circuits in the above literature is that the simulation actually needs a lot of calculations, so optimization of the parameters takes a very long time. ANN has been chosen as an alternative method to design microwave circuits and devices, hence ANNs have been used to design circular and rectangular resonators modelled in SIW technology [26, 27]. A back-propagation neural network-based approach for modelling the SIW power dividers has been proposed [28]. In order to model and optimize the microwave components and devices, an efficient hybrid sampling method has been proposed to get optimum design parameters by using the ANN model [29].

The main contribution of the proposed research work is a feed forward multilayer perceptron (FF-MLP) neural network that has been used to optimize the proposed filter parameters. In this work, two networks with $2 \times 12 \times 1$ and $1 \times 8 \times 1$ have been used. The trainlm function in MATLAB has been used to efficiently train the FF-MLP neural networks. The S_{11} parameter has been calculated to evaluate the proposed networks, and the results obtained are in good agreement with the simulated results. Instead of a single CSRR, two CSRRs have been employed to enhance the proposed band pass filter's roll-off rate.

This paper is organized as follows. Section 2 explains how the basic topology of the proposed SIW filter is designed. Section 3 explains how the filter parameters are optimized using neural networks. Section 4 shows how the filter was simulated and the simulation results. Section 5 provides the fabrication process, measurement setup, and the measured results plotted against the simulated ones.

2. DESIGN OF CROSS SHAPED SIW CAVITY WITH CSRR

The proposed cross shaped SIW cavity topology is depicted in Figure 1. The basic SIW topology consists of three layers. The perfect electric conductor (PEC) is used as bottom layer and top layer, and the middle layer is dielectric material. The dielectric material used is Roggers RO4003C with dielectric constant $\varepsilon_r = 3.55$ and height of the substrate $h = 0.81\,\text{mm}$. The optimized design dimensions of this SIW cavity are as follows. The length of the SIW cavity is $L = 40.8\,\text{mm}$; the length of the dielectric substrate used is $L_{sub} = 60\,\text{mm}$; the feeding slot length $L_{slot} = 5.4\,\text{mm}$; the feeding slot width $W_{gap} = 1.4\,\text{mm}$; the width of the microstrip line is $W_{mst} = 2\,\text{mm}$; the diameter of the metallic post or via-hole is $d = 1.2\,\text{mm}$. These metallic posts are placed with two different allowable separation distances or pitches (via-to-via distance) of the vias $p = 1.7\,\text{mm}$ and $p_1 = 2\,\text{mm}$. The geometries of this cross shaped SIW cavity in horizontal and vertical directions are the same.

2.1. Design of CSRR

The square shape CSRR is used in the filter design process, and the physical appearance of this CSRR is as depicted in Figure 2. The CSRR acts as an electric dipole, and this CSRR structure is etched on the upper PEC of the SIW cavity. The exited mode of the CSRR is the same as the dominant mode TE_{10} of the SIW cavity.

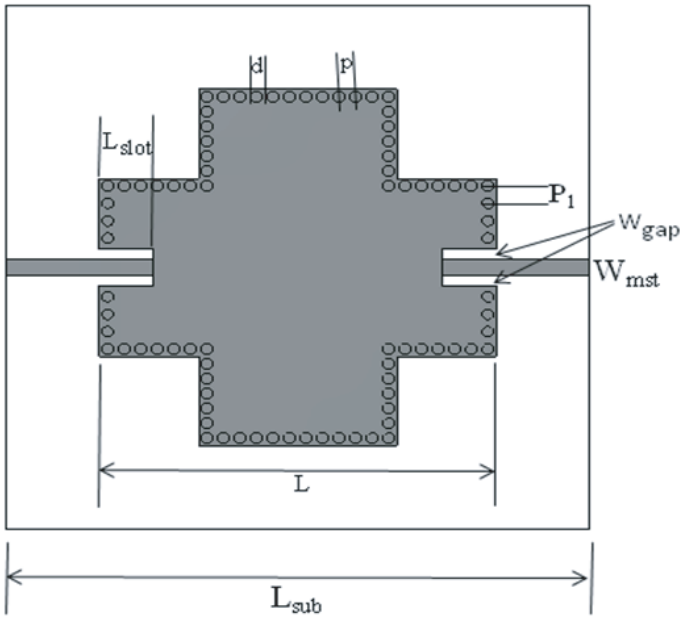

Figure 1. Cross shaped SIW cavity.

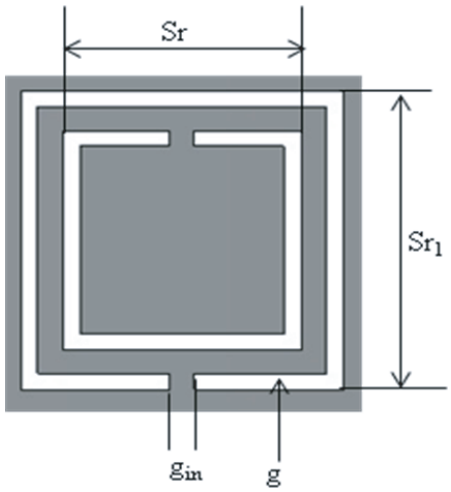

Figure 2. Structure of CSRR.

The CSRR structure resembles an LC resonant circuit. The resonance frequency of the CSRR is computed by the self inductance L and capacitance per unit length C'. The resonant frequency of square shaped CSRR is given by [16]

$$f_r = \frac{1}{2\pi\sqrt{L_0 C_0}} \tag{1}$$

where L_0 and C_0 represent the equivalent inductance and equivalent capacitance of the CSRR structure. The equivalent capacitance C_0 can be derived by using the following expression,

$$C_0 = (C_s + C_g)/2 \tag{2}$$

where C_s and C_g are series and gap capacitances of CSRR, and these two capacitances can be found by using some of the SIW filter parameters like width (w), metal thickness (mt), and free space permittivity (ε_0). In this paper, by using these square shaped CSRRs two SIW bandpass filters are designed.

2.2. SIW Bandpass Filter with Single CSRR

Initially an SIW bandpass filter with single CSRR is designed and fabricated. This design process is done by using SIW crosses shaped topology with the optimized values which have already been mentioned earlier, and then CSRR is loaded into it. The CSRR is etched on the top layer of the structure which is a conducting material (PEC), with the optimized geometrical parameters as follows, $S_r = 2.8\,\text{mm}$, $S_{r1} = 3.8\,\text{mm}$, $g = 0.4\,\text{mm}$, $g_{in} = 0.4\,\text{mm}$, and this total topology is as shown in Figure 3 which is designed and simulated using CST microwave studio. The fabricated prototype model is shown in Figure 9(a).

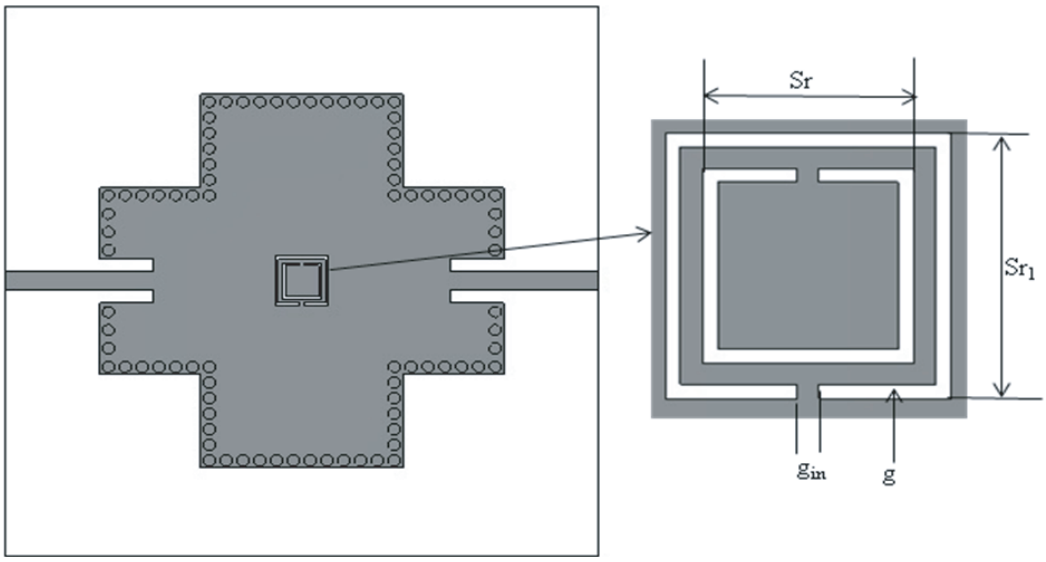

Figure 3. SIW bandpass filter with single CSRR.

2.3. SIW Bandpass Filter with two CSRRs

Another SIW bandpass filter is designed with two CSRR rings facing each other with a separation distance $t = 0.6\,\text{mm}$, and it was fabricated. The optimized values are: $d = 1.2\,\text{mm}$, $L_{sub} = 60\,\text{mm}$, $L = 40.8\,\text{mm}$, $L_{slot} = 5.6\,\text{mm}$, $p = 1.7\,\text{mm}$, $p_1 = 2\,\text{mm}$, $W_{mst} = 1.6\,\text{mm}$, $W_{gap} = 1.4\,\text{mm}$.

Now in this topology two CSRRs are etched on the upper conducting layer (PEC), with the optimized geometrical parameters as follows, $S_r = 2.6\,\text{mm}$, $S_{r1} = 3.4\,\text{mm}$, $g = 0.4\,\text{mm}$, $g_{in} = 0.4\,\text{mm}$, as shown in Figure 4 and designed and simulated using CST microwave studio, and the fabricated prototype model is shown in Figure 9(b).

3. ANN OPTIMIZATION

3.1. Typical Structure of the Artificial Neural Networks (ANN)

The basic structure of ANN shown in Figure 5 consists of three sections. The first section is the input layer; the second section is hidden layer which has one or more sub-layers; and the third section is the output layer. In each stage, there are some processing units which are known as neurons, and all these neurons are interconnected to each other. Each neuron receives some information from one or more other neurons and is processed further. The neural network produces an output which is a weighted sum of all the information from input layer and hidden layer. There are several types of neural networks, which are categorized based on the neuron types and the interconnections between them.

The input to the neurons in the input layer is externally (out of the neural network) applied. The output of the input layer neurons acts as input to the hidden layer neurons. The information is processed

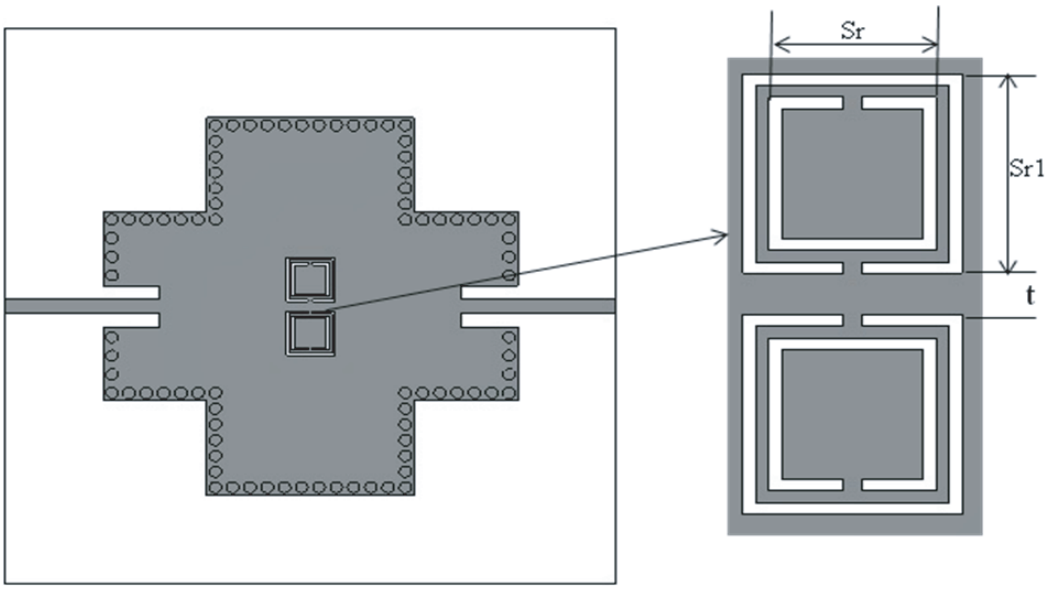

Figure 4. SIW bandpass filter with two CSRRs.

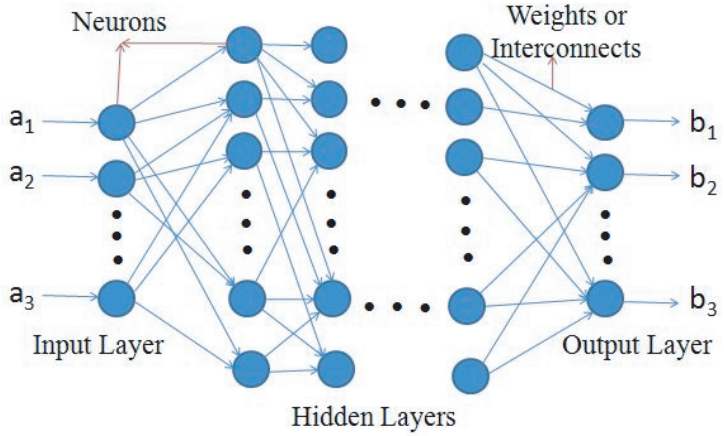

Figure 5. Topology of MLP-ANN.

among all these hidden layer neurons, and finally the output of the hidden layer acts as input to the output layer.

3.2. Filter Parameters Optimization Using ANN

The physical parameters of the proposed filter are optimised by using ANN in MATLAB. Basically there are many types of neural networks. Among them, FF-MLP neural network is used for the optimization of proposed filter parameters.

3.2.1. Neural Network Training

The S_{11} output data collected from the parametric analysis in CST are used as training data, shown in Table 1 and Table 2. Two neural networks are designed to optimize the filter parameters. The first network contains one input layer with two neurons, one hidden layer with 12 neurons, and one output layer with one neuron. In order to train the first network, the data shown in Table 1 are used. The filter

Table 1. Training data for first network.

S. No.	S_r (mm)	S_{r1} (mm)	S_{11} (dB) (CST)
1	2.05	3.05	−8.542
2	2.15	3.15	−10.853
3	2.25	3.25	−11.101
4	2.35	3.35	−11.780
5	2.45	3.45	−12.676
6	2.55	3.55	−13.967
7	2.65	3.65	−16.712
8	2.75	3.75	−20.083
9	2.85	3.85	−23.397
10	2.95	3.95	−18.860
11	3.05	4.05	−18.643

Table 2. Training data for second network.

S. No.	W_{gap} (mm)	S_{11} (dB) (CST)
1	0.75	−11.137
2	0.85	−13.165
3	0.95	−14.766
4	1.05	−16.181
5	1.15	−17.911
6	1.25	−19.915
7	1.35	−22.001
8	1.45	−23.268
9	1.55	−22.185

parameters S_r and S_{r1} are applied to the input layer, and S_{11} is the target value. The second network also consists of one input layer with single neuron, one hidden layer with 8 neurons, and the output layer with one neuron, and it is trained with the data shown in Table 2. The second network is used to optimize the filter parameter W_{gap}. These two neural networks are trained using Levenberg Marquart (LM) algorithm, for which the 'trainlm' function is used, and log-sigmoid is used as transformation function. Adaption learning function (LEARNGDM) is used with a learning rate of 0.01.

The training of this neural network is carried out with a learning method known as supervised learning error back propagation method. In this method, the mean square error is back propagated, and the weights are updated accordingly in order to get minimum error. After training the network with the sample data, the weights of this network remain constant, and the neural network is enough trained. Now the neural network is ready to examine with the testing data.

3.2.2. Neural Network Testing

After enough training, the neural network is ready for testing with the data shown in Table 3 and Table 4, and the final results are also included in the same table. The testing dada and the S_{11} obtained in CST MWS agree well with each other with minimum mean square error.

Table 3. Testing data for first network.

S. No.	S_r (mm)	S_{r1} (mm)	S_{11} (dB) (CST)	S_{11} (dB) (ANN)
1	2.0	3.0	−6.441	-6.5070
2	2.1	3.1	−10.646	−10.5359
3	2.2	3.2	−11.057	−10.8425
4	2.3	3.3	−11.435	−11.2598
5	2.4	3.4	−12.89	−12.9872
6	2.5	3.5	−13.226	−13.3160
7	2.6	3.6	−14.618	−14.7271
8	2.7	3.7	−18.247	−18.3683
9	2.8	3.8	−24.095	−23.9871
10	2.9	3.9	−23.851	−23.8316
11	3.0	4.0	−23.359	−22.7611
12	3.1	4.1	−21.844	−21.9474

Table 4. Testing data for second network.

S. No.	W_{gap} (mm)	S_{11} (dB) (CST)	S_{11} (dB) (ANN)
1	0.8	−12.515	−12.6186
2	0.9	−13.997	−13.7384
3	1.0	−15.505	−15.5065
4	1.1	−17.054	−17.0542
5	1.2	−18.975	−18.4913
6	1.3	−20.912	−20.9320
7	1.4	−23.782	−23.7203
8	1.5	−23.125	−23.5102
9	1.6	−22.344	−22.3218

4. RESULTS AND DISCUSSION

The simulated results are as shown in Figure 6. Figure 6(a) shows the transmission characteristics of the SIW cavity filter with single CSRR slot, which was designed and simulated using CST microwave studio. From the graph it is clear that there are two closely spaced resonances observed at 8.4 GHz and 8.6 GHz, with the passband centre frequency of 8.5 GHz. Significantly one of the resonant frequencies is caused by the CSRR, and the other resonant frequency is because of the SIW cavity. The proposed filter offers a good reflection which is better than −10 dB, and the reflection bandwidth is 485 MHz, from 8.29 to 8.77 GHz. The transmission bandwidth at −1 dB is 480 MHz, and it is between 8.3 GHz and 8.78 GHz. At −3 dB, the transmission bandwidth is 730 MHz, and it is from 8.22 GHz to 8.95 GHz. Within the frequency range from 8.38 to 8.64 GHz, the return loss is smaller than −24 dB.

Figure 6(b) presents the transmission characteristics of proposed SIW band pass filter with two CSRR slots. At −1 dB, the bandwidth obtained is 410 MHz, ranging from 8.27 to 8.68 GHz, and the bandwidth considered at −3 dB is 530 MHz, which is from 8.21 to 8.73 GHz, with the centre frequency of 8.5 GHz. This filter also shows two resonant frequencies, one at 8.38 GHz and the other at 8.62 GHz. At −10 dB, the reflection bandwidth is 460 MHz, from 8.26 to 8.72 GHz. Two proposed filters show an insertion loss about −0.5 dB and −0.8 dB within the passband region. These filters show high out of band rejection in lower and higher frequency ranges. The first filter shows a transmission zero at

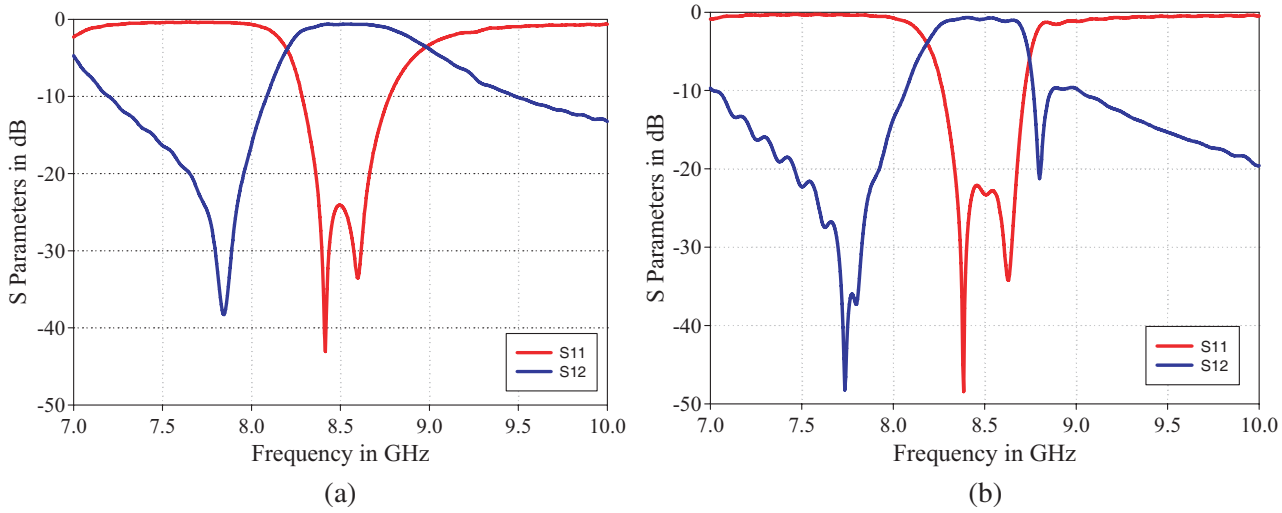

Figure 6. (a) S_{11} and S_{12} of filter with single CSRR. (b) S_{11} and S_{12} of filter with two CSRR.

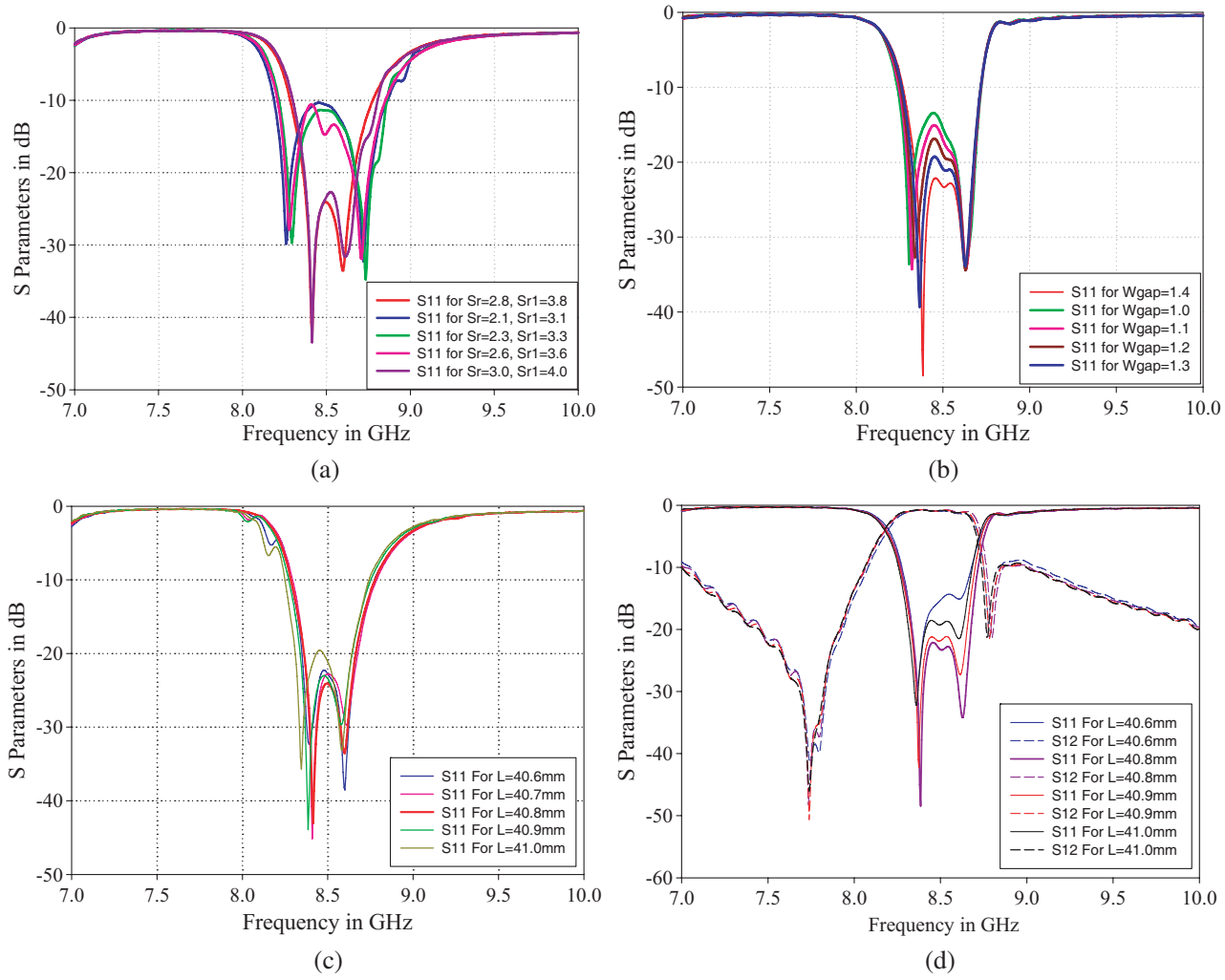

Figure 7. (a) parametric response w.r.t S_r and S_{r1}. (b) Parametric response w.r.t W_{gap}. (c) & (d) Parametric response w.r.t L for both the filters.

7.85 GHz which is introduced by single CSRR slot, and the second filter shows two transmission zeros at 7.73 GHz and 8.8 GHz, because of two CSRR slots. In order to increase the roll-off rate of the band pass filter, two CSRRs have been used instead of single CSRR.

4.1. Parametric Analysis

A set of training data required to train the neural network is generated from the parametric analysis of both the filters, and the corresponding parametric plots are depicted in Figure 7. This analysis was carried out by changing different parameters of these filters like S_r, S_{r1}, W_{gap}, and L.

4.2. E-Field Distribution

Figures 8(a) and 8(b) show the electric field distribution of filters with single CSRR and two CSRRs, respectively. The electric field strength of the proposed filters is indicated by the vertical colour ramps (right side of Figures 8(a) and 8(b)). The red colour shifts on the upper surface of the filters represent the growth of the electric field strength. The proposed CSRRs incorporated SIW filters show the TE_{10} (dominant mode) behaviour like conventional rectangular waveguide.

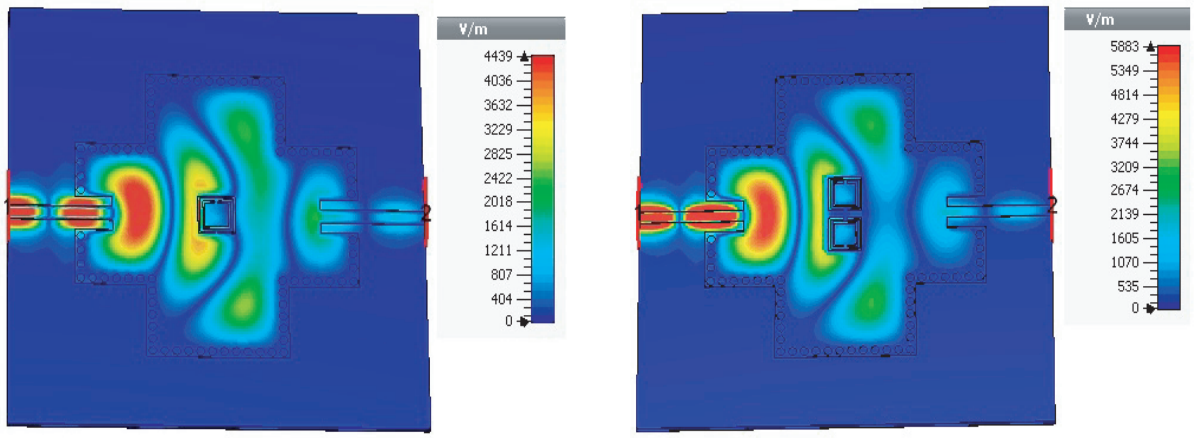

(a) (b)

Figure 8. (a) Electric field distribution of filter with single CSRR. (b) Electric field distribution of filter with two CSRRs.

5. FABRICATION AND PRACTICAL VALIDATION

The proposed filters are fabricated, and the top views of the two prototype models are shown in Figures 9(a)–9(b), and the back view is shown in Figure 9(c) with dimensions mentioned above. Rogers RO4003C is used as the dielectric substrate with a relative permittivity of $\varepsilon_r = 3.55$ and loss tangent of $\tan\delta = 0.0027$, and the height of the substrate is $h = 0.81$ mm. The fabrication was done by using the standard PCB process. At the initial stage of fabrication, copper metal is used to coat either side of the substrate material. Vias are drilled in order to form the SIW structure, and these vias are coated with copper metal. In the final stage of fabrication, the CSRR slots are etched on the upper PEC as shown in Figure 9. The measurement of prototype models is carried out with the help of Combinational Analyzer (Anritsu-MS2037C), and the measurement setup is shown in Figure 10.

The measured results are compared with the simulated ones as shown in Figure 11, and they are in good agreement. From Figure 11(a) and Figure 11(b), at -10 dB it is observed that the measured S_{11} is shifted by 50 MHz (from 8.28 to 8.33 GHz) and 70 MHz (from 8.26 to 8.33 GHz) respectively from simulated S_{11}, and at the centre frequency (8.5 GHz), measured S_{12} is shifted by 0.41 dB and 1 dB respectively from the simulated S_{12}. The slight mismatch in results is due to the fabrication tolerances, and this deviation is also because SMA connecters are not taken into account while the simulation is

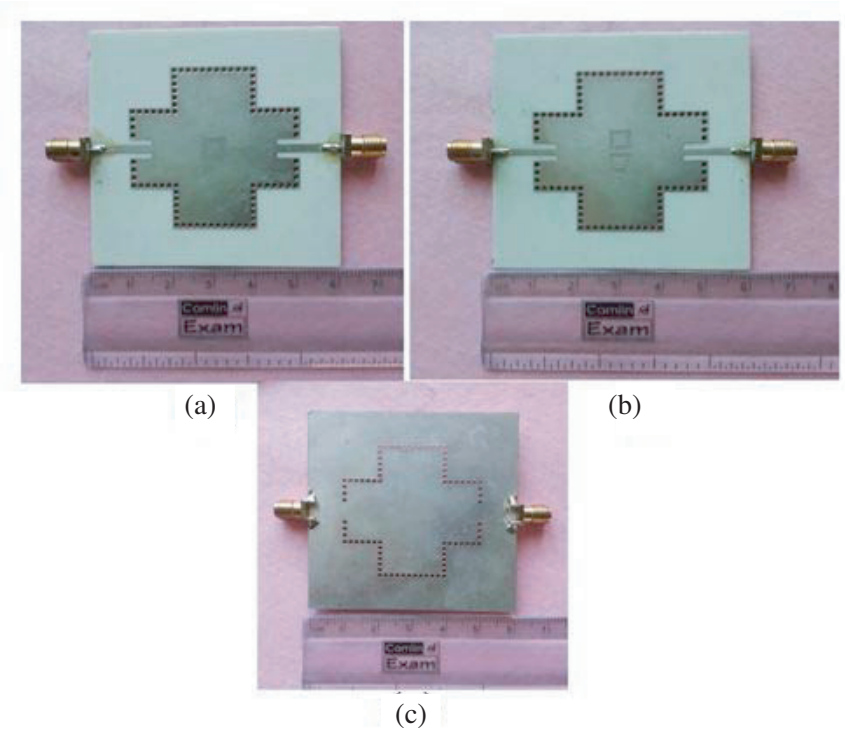

Figure 9. Fabrication models of SIW BPF. (a) With single CSRR. (b) With two CSRRs. (c) Back view.

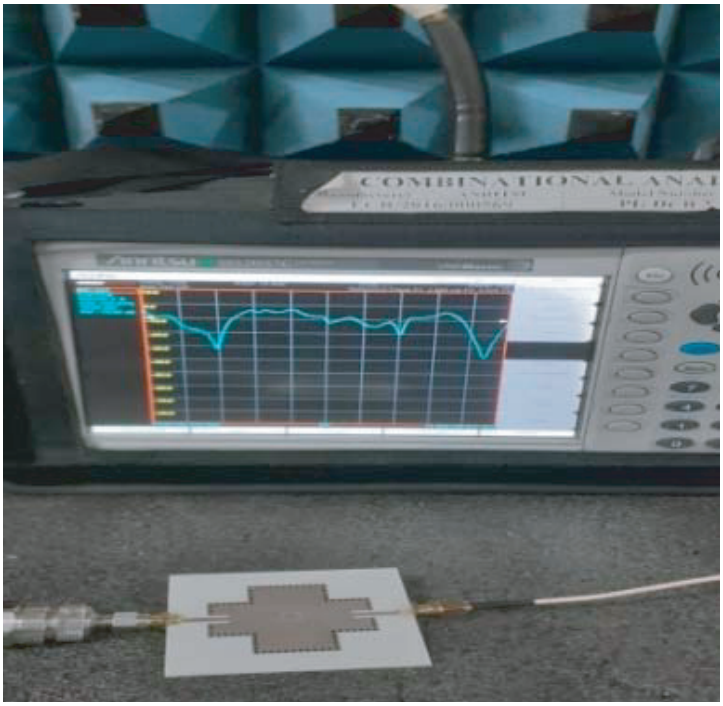

Figure 10. Measurement setup.

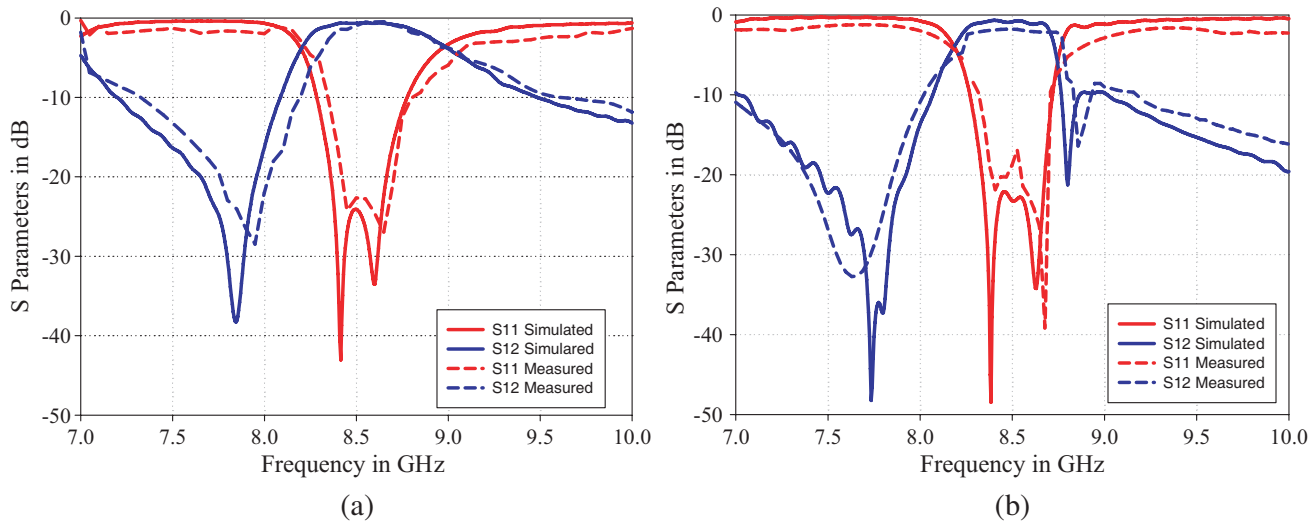

Figure 11. Simulated and Measured results of (a) BPF with single CSRR, (b) BPF with two CSRRs.

performed. At the passband centre frequency, the two results show better than −22 dB and −18 dB return losses, respectively.

The performance parameters of the proposed bandpass filters, such as passband center frequency, insertion loss, fractional bandwidth, return loss, dielectric substrate, and type of technique used have been compared with the previous literature and are summarized in Table 5. From Table 5 it is clear that the proposed filters provide better insertion loss, fractional bandwidth, and return loss.

Table 5. Comparison of proposed filters with similar bandpass filters.

Ref. No.	f_0 (GHz)	IL (dB)	FBW (%)	S_{11} (dB)	Substrate (ε_r)	Technique
[15]	3.5	1.45	6	−20	Taconic RF-30(3)	CSRR
[19]	5	≈ 2	3.2	−16.6	Roggers RT Duroid 5880(2.2)	CSRR
[23]	2.4	1.25	10.5	−20	Roggers RO4003C(3.55)	FOCSRR
[24]	5.8	0.9	8.5	−22	Roggers RT Duroid 5880(2.2)	CORR
[25] (Measured)	15	1.7	4.3	≈ −20	Roggers RT Duroid 5880(2.2)	—
This work Filter I	8.5	0.5	8.5	−24	Roggers RO4003C(3.55)	CSRR, ANN
Filter II	8.5	0.8	6.1	−23	Roggers RO4003C(3.55)	CSRR, ANN

f_0 = Pass band center frequency; IL = Insertion Loss; FBW = Fractional bandwidth.
Filter I: SIW bandpass filter with single CSRR
Filter II: SIW bandpass filter with two CSRRs

6. CONCLUSION

Two bandpass filters based on SIW with CSRRs are implemented with the help of an FF-MLP neural network. The neural network is trained properly, and the parameters S_r, S_{r1}, and W_{gap} are optimized. The prototypes of proposed filter configurations are fabricated using PCB combined with plated through hole technology, and the measured results are in good agreement with the simulated results and neural network optimized results. The measured reflection coefficients for the two filters are -22 dB and -18 dB, respectively, and the insertion losses are -1 dB and -3 dB, respectively. The computational time of the neural network is very low compared to the full wave simulations performed with CST microwave studio. The mean square error measured between simulated and neural network results is almost negligible. Hence, the FF-MLP neural network with LM algorithm is one of the best parameter optimization techniques, compared to other commercial software.

ACKNOWLEDGMENT

Authors would to thank KL University, Guntur, Andhra Pradesh, India for providing the measurement facilities. Sincere thanks to Dr. V. Krushna Kanth for the valuable technical discussions.

REFERENCES

1. Deslandes, and K. Wu, "Single-substrate integration technique of planar circuits and Waveguide filters," *IEEE Transactions on Microwave Theory and Techniques*, Vol. 51, No. 2, 593–596, 2003.
2. Khorand, T. and M. S. Bayati, "Novel half-mode substrate integrated waveguide bandpass filters using semi-hexagonal resonators," *International Journal of Electronics and Communications (AEU)*, Vol. 95, 52–58, 2018.
3. Ananya, P., P. Athira, and S. Raghavan, "Miniaturized band pass filter in substrate integrated waveguide technology," *International Journal of Engineering & Technology*, Vol. 7, No. 3.13, 95–98, 2018.
4. Ananya, P., P. Athira, and S. Raghavan, "Miniaturizing SIW filters with SLOW-wave technique," *AEU — Int. J. Electron. Commun.*, Vol. 84, 360–365, 2018.
5. Bozzi, M., G. Apostolos, and K. Wu, "Review of substrate-integrated waveguide circuits and antennas," *Microwaves, Antennas & Propagation*, Vol. 5, 909–920, IET, 2011.
6. Krushna Kanth, V. and S. Raghavan, "EM design and analysis of a substrate integrated waveguide based on a frequency-selective surface for millimeter wave radar application," *J. Comput. Electron.*, Vol. 18, 189–196, 2019.
7. Krushna Kanth, V. and R. Singaravelu, "Design of a hybrid A-sandwich radome using a strongly coupled frequency selective surface element," *International Journal of Microwave and Wireless Technologies*, Vol. 12, No. 8, 738–748, 2020.
8. Krushna Kanth, V. and R. Singaravelu, "Design and implementation of 2.5D frequency selective surface based on substrate integrated waveguide technology," *International Journal of Microwave and Wireless Technologies*, Vol. 11, No. 3, 255–267, 2019.
9. Tomassoni, C., L. Silvestri, M. Bozzi, and L. Perregrini, "Substrate-integrated waveguide filters based on mushroom-shaped resonators," *International Journal of Microwave and Wireless Technologies*, Vol. 8, No. 4–5, 741–749, 2016.
10. Chen, C. and J. Qin, "Triple-mode dual-band bandpass filter based on cross-shaped substrate integrated waveguide," *Electronics Letters*, Vol. 55, No. 3, 138–140, 2018.
11. Xu, J., J. J. Bi, Z. L. Li, and R. S. Chen, "Optimization of SIW band-pass filter with wide and sharp stopband using space mapping," *International Journal of Electronics*, Vol. 103, No. 12, 2042–2051, 2016.
12. Aghayari, H., N. Komjani, and N. M. Garmjani, "A novel H plane filter using double-layer substrate integrated waveguide with defected ground structures," *International Journal of Electronics*, Vol. 100, No. 6, 851–862, 2013.

13. Chaudhury, S. S., S. Awasthi, and R. K. Singh, "Dual band bandpass filter based on substrated integrated waveguide loaded with mushroom resonators," *Microw. Opt. Technol. Lett.*, Vol. 62, 2226–2235, 2020.
14. Chen, L.-N., Y.-C. Jiao, Z. Zhang, and F.-S. Zhang, "Miniaturized substrate integrated waveguide dual-mode filters loaded by a series of cross-slot structures," *Progress In Electromagnetics Research C*, Vol. 29, 29–39, 2012.
15. Zhang, Q., W. Yin, S. He, and L. Wu, "Compact Substrate Integrated Waveguide (SIW) bandpass filter with Complementary Split-Ring Resonators (CSRRs)," *IEEE Microwave and Wireless Components Letters*, Vol. 20, No. 8, 426–428, 2010.
16. Li, W., Z. Tang, and X. Cao, "Design of a SIW bandpass filter using defected ground structure with CSRRs," *Active and Passive Electronic Components*, 6 pages, 2017.
17. Wu, L., X. Zhou, Q. Wei, and W. Yin, "An extended doublet Substrate Integrated Waveguide (SIW) bandpass filter with a Complementary Split Ring Resonator (CSRR)," *IEEE Microwave and Wireless Components Letters*, Vol. 19, No. 12, 777–779, 2009.
18. Dong, D., T. Yang, and T. Itoh, "Substrate integrated waveguide loaded by complementary split-ring resonators and its applications to miniaturized waveguide filters," *IEEE Transactions on Microwave Theory and Techniques*, Vol. 57, No. 9, 2211–2223, 2009.
19. Pu, J., F. Xu, and Y. Li, "Miniaturized substrate integrated waveguide bandpass filters based on novel complementary split ring resonators," *IEEE MTT-S International Microwave Biomedical Conference (IMBioC)*, Nanjing, China, 2019.
20. Jiang, W., W. Shen, L. Zhou, and W.-Y. Yin, "Miniaturized and highselectivity Substrate Integrated Waveguide (SIW) bandpass filter loaded by Complementary Split-Ring Resonators (CSRRs)," *Journal of Electromagnetic Waves and Applications*, Vol. 26, No. 11–12, 1448–1459, 2012.
21. Park, W.-Y. and S. Lim, "Miniaturized half-mode substrate integrated waveguide bandpass filter loaded with double-sided complementary split-ring resonators," *Electromagnetics*, Vol. 32, No. 4, 200–208, 2012.
22. Huang, L., I. D. Robertson, N. Yuan, and J. Huang, "Novel substrate integrated waveguide bandpass filter with broadside-coupled complementary split ring resonators," *IEEE/MTT-S International Microwave Symposium Digest*, Montreal, QC, Canada, 2012.
23. Ghayoumi Zadeh, H. and M. Danaeian, "Miniaturized substrate integrated waveguide filter using fractal open complementary split-ring resonators," *International Journal of RF and Microwave Computer-Aided Engineering*, Vol. 28, 2018.
24. Yan, T., X.-H. Tang, Z.-X. Xu, and D. Lu, "A novel type of bandpass filter using complementary open-ring resonator loaded HMSIW with an electric cross-coupling," *Microwave and Optical Technology Letters*, Vol. 58, 998–1001, 2016.
25. Chu, P., et al., "Dual-mode substrate integrated waveguide filter with flexible response," *IEEE Transactions on Microwave Theory and Techniques*, Vol. 65, No. 3, 824–830, March 2017.
26. Angiulli, G., E. Arnieri, D. De Carlo, and G. Amendola, "Feed forward neural network characterization of circular SIW resonators," *IEEE Antennas and Propagation Society International Symposium*, San Diego, CA, USA, 2008.
27. Amendola, G., G. Angiulli, E. Arnieri, L. Boccia, and D. De Carlo, "Characterization of lossy SIW resonators based on multilayer perceptron neural networks on graphics processing unit," *Progress In Electromagnetics Research C*, Vol. 42, 1–11, 2013.
28. Li, J. and T. Dong, "Design of a substrate integrated waveguide power divider that uses a neural network," *2nd International Conference on Computer Engineering and Technology*, Chengdu, China, 2010.
29. Zhang, Z., Q. S. Cheng, H. Chen, and F. Jiang, "An efficient hybrid sampling method for neural network-based microwave component modeling and optimization," *IEEE Microwave and Wireless Components Letters*, Vol. 30, No. 7, 625–628, 2020.